
Loss Surfaces, Mode Connectivity, and Fast Ensembling of DNNs

Timur Garipov^{*1} Pavel Izmailov^{*2} Dmitrii Podoprikin^{*1} Dmitry Vetrov³ Andrew Gordon Wilson²

Abstract

The loss functions of deep neural networks are complex and their geometric properties are not well understood. We show that the optima of these complex loss functions are in fact connected by a simple curves, such as a polygonal chain with only one bend, over which training and test accuracy are nearly constant. We introduce a training procedure to discover these high-accuracy pathways between modes. Inspired by this new geometric insight, we also propose a new ensembling method entitled Fast Geometric Ensembling (FGE). Using FGE we can train high-performing ensembles in the time required to train a single model. We achieve improved performance compared to the recent state-of-the-art Snapshot Ensembles, on CIFAR-10 and CIFAR-100, using state-of-the-art deep residual networks. On ImageNet we improve the top-1 error-rate of a pre-trained ResNet by 0.56% by running FGE for just 5 epochs.

1. Introduction

The loss surfaces of deep neural networks (DNNs) are highly non-convex and can depend on millions of parameters. The geometric properties of these loss surfaces are not well understood. Even for simple networks, the number of local optima and saddle points is large and can grow exponentially in the number of parameters (Auer et al., 1996; Dauphin et al., 2014; Choromanska et al., 2015). Moreover, the loss is high along a line segment connecting two optima (e.g., Goodfellow et al., 2015; Keskar et al., 2017). These two observations suggest that the local optima are isolated.

In this paper, we provide a new training procedure which can in fact find paths of near-constant accuracy between the modes of large deep neural networks. Furthermore, we show that for a wide range of architectures we can find these paths in the form of a simple polygonal chain of two line segments. Consider, for example, Figure 1, which illus-

trates the ResNet-164 L_2 -regularized cross-entropy loss on CIFAR-100, through three different planes. The left panel shows all affine combinations of the weights of three independently trained networks. In this plane, all optima are isolated, which corresponds to the standard intuition. However, the middle and right panels show two different paths of near-constant accuracy between the modes in weight space, discovered by our proposed training procedure. The endpoints of these paths are the two independently trained DNNs corresponding to the two lower modes on the left panel.

We believe that this geometric discovery has major implications for research into multilayer networks, including (1) improving the efficiency, reliability, and accuracy of training, (2) creating better ensembles, and (3) deriving more effective posterior approximation families in Bayesian deep learning. Indeed, in this paper we are inspired by this geometric insight to propose a new ensembling procedure that can efficiently discover multiple high-performing but diverse deep neural networks.

In particular, our contributions include:

- A new method that finds paths between two local optima, such that the train loss and test error remain low along these paths.
- Using the proposed method we demonstrate that such mode connectivity holds for several deep neural networks, on key benchmarks such as CIFAR-100.
- We show that these paths do not merely exist due to overparametrization, but instead correspond to meaningfully different representations, which can be efficiently ensembled for increased accuracy.
- Inspired by these observations, we propose Fast Geometric Ensembling (FGE), which outperforms existing ensembling techniques, including the recent Snapshot Ensembles (Huang et al., 2017), on CIFAR-10 and CIFAR-100, using state-of-the-art deep neural networks such as VGG-16, Wide ResNet-28-10, and ResNet-110. On ImageNet we achieve 0.56% top-1 error-rate improvement for a pretrained ResNet-50 model by running FGE for 5 epochs.

^{*}Equal contribution ¹Moscow State University ²Cornell University ³Higher School of Economics. Correspondence to: Andrew Gordon Wilson <andrew@cornell.edu>.

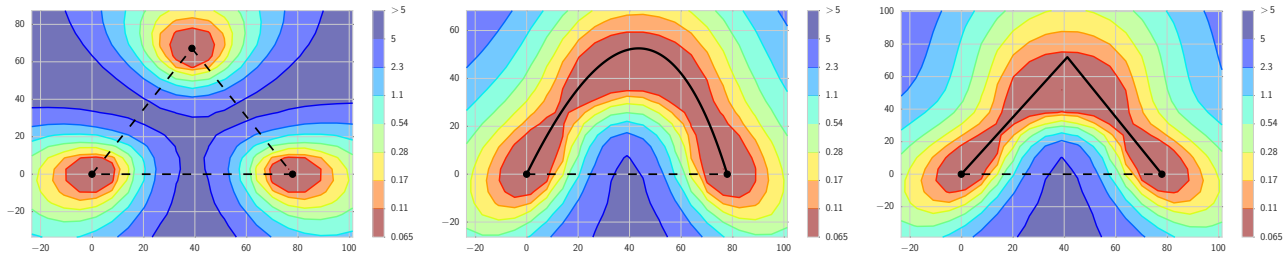


Figure 1. The cross-entropy loss surface of a deep residual network (ResNet-164) on CIFAR-100, as a function of network weights in a two-dimensional subspace. In each panel, the horizontal axis is fixed and is attached to the optima of two independently trained networks. The vertical axis changes between panels as we change planes. **Left:** Three optima for independently trained networks. **Middle and Right:** A quadratic Bezier curve, and a polygonal chain with one bend, connecting the lower two optima on the left panel along a path of near-constant loss. Notice that in each panel a direct linear path between each mode would incur high loss.

The rest of the paper is organized as follows. Section 2 discusses existing literature on DNN loss geometry and ensembling techniques. Section 3 introduces the proposed method to find the curves with low train loss and test error between local optima, which we investigate empirically in section 4. Section 5 then introduces our proposed ensembling technique, FGE, which we empirically compare to the alternatives in section 6. Finally, in section 7 we discuss connections to other fields and directions for future work.

Note that we interleave two sections where we make methodological proposals (sections 3, 5), with two sections where we perform experiments (sections 4, 6).

2. Related Work

Despite the success of deep learning across many application domains, the loss surfaces of deep neural networks are not well understood. These loss surfaces are an active area of research, which falls into two distinct categories.

The first category explores the local structure of minima found by SGD and its modifications. Researchers typically distinguish sharp and wide local minima, which are respectively found by using large and small mini-batch sizes during training. Hochreiter & Schmidhuber (1997) and Keskar et al. (2017), for example, claim that flat minima lead to strong generalization, while sharp minima deliver poor results on the test dataset. However, recently Dinh et al. (2017) argue that most existing notions of flatness cannot directly explain generalization. To better understand the local structure of DNN loss minima, Li et al. (2017) proposed a new visualization method for the loss surface near the minima found by SGD. Applying the method for a variety of different architectures, they showed that the loss surfaces of modern residual networks are seemingly smoother than those of VGG-like models.

The other major category of research considers global loss structure. One of the main questions in this area is how

neural networks are able to overcome poor local optima. Choromanska et al. (2015) investigated the link between the loss function of a simple fully-connected network and the Hamiltonian of the spherical spin-glass model. Under strong simplifying assumptions they showed that the values of the investigated loss function at local optima are within a well-defined bound. In other research, Lee et al. (2016) showed that under mild conditions gradient descent almost surely converges to a local minimizer and not a saddle point, starting from a random initialization.

In recent work Freeman & Bruna (2017) theoretically showed that local minima of a neural network with one hidden layer and ReLU activations can be connected with a curve such that the loss is upper-bounded along the curve by a constant that depends on the number of parameters of the network and the “smoothness of the data”. Using a dynamic programming approach they were able to construct a polygonal chain for AlexNet on CIFAR-10 such that the test accuracy stays above 80% along the curve. The polygonal chain they constructed needed to have at least 6 bends.

By contrast, we propose a much simpler training procedure that can find near-constant accuracy polygonal chains with only 1 bend between optima, even with modern state-of-the-art architectures. Inspired by properties of the loss function discovered by this procedure, we also propose a new state-of-the-art ensembling method that can be trained in the time required to train a single DNN.

Xie et al. (2013) proposed a related ensembling approach that gathers outputs of neural networks from different epochs at the end of training to stabilize final predictions. More recently, Huang et al. (2017) proposed *snapshot ensembles*, which use a cosine cyclical learning rate (Loshchilov & Hutter, 2016) to save “snapshots” of the model during training at times when the learning rate achieves its minimum. In our experiments, we compare our geometrically inspired approach to Huang et al. (2017), showing improved performance.

Draxler et al. (2018) simultaneously and independently discovered the existence of curves connecting local optima in DNN loss landscapes. To find these curves they used a different approach inspired by the *Nudged Elastic Band* method (Jonsson et al., 1998) from quantum chemistry.

3. Finding Paths between Modes

We describe a new method to minimize the training error along a path that connects two points in the space of DNN weights. Section 3.1 introduces this general procedure for arbitrary parametric curves, and section 3.2 describes polygonal chains and Bezier curves as two example parametrizations of such curves. We then describe in section 3.3 how to apply batch normalization at test time to points on these curves. In the supplementary material, we discuss the computational complexity of the proposed approach.

3.1. Connection Procedure

Let \hat{w}_1 and \hat{w}_2 in $\mathbb{R}^{|\text{net}|}$ be two sets of weights corresponding to two neural networks independently trained by minimizing any user-specified loss $\mathcal{L}(w)$, such as the cross-entropy loss. Here, $|\text{net}|$ is the number of weights of the DNN. Moreover, let $\phi_\theta : [0, 1] \rightarrow \mathbb{R}^{|\text{net}|}$ be a continuous piecewise smooth parametric curve, with parameters θ , such that $\phi_\theta(0) = \hat{w}_1$, $\phi_\theta(1) = \hat{w}_2$.

To find a path of high accuracy between \hat{w}_1 and \hat{w}_2 , we propose to find the parameters θ that minimizes the expectation over a uniform distribution on the curve, $\hat{\ell}(\theta)$:

$$\hat{\ell}(\theta) = \frac{\int \mathcal{L}(\phi) d\phi}{\int d\phi} = \frac{\int_0^1 \mathcal{L}(\phi(t)) \|\phi'(t)\| dt}{\int_0^1 \|\phi'(t)\| dt}. \quad (1)$$

The numerator of (1) is the line integral of the loss \mathcal{L} on the curve, and the denominator $\int_0^1 \|\phi'(t)\| dt$ is the normalizing constant of the uniform distribution on the curve defined by $\phi(\cdot)$. This proposed loss can be rewritten as an expectation

$$\hat{\ell}(\theta) = \int_0^1 \mathcal{L}(\phi_\theta(t)) q_\theta(t) dt = \mathbb{E}_{t \sim q_\theta(t)} [\mathcal{L}(\phi_\theta(t))], \quad (2)$$

where the distribution $q_\theta(t)$ on $t \in [0, 1]$ is defined as:

$$q_\theta(t) = \left(\int_0^1 \|\phi'_\theta(t)\| dt \right)^{-1} \|\phi'_\theta(t)\|.$$

Stochastic gradients of $\hat{\ell}(\theta)$ in Eq. (2) are generally intractable since $q_\theta(t)$ depends on θ . Therefore we also pro-

pose a more computationally tractable loss

$$\ell(\theta) = \int_0^1 \mathcal{L}(\phi_\theta(t)) dt = \mathbb{E}_{t \sim U(0,1)} \mathcal{L}(\phi_\theta(t)), \quad (3)$$

where $U(0, 1)$ is the uniform distribution on $[0, 1]$. The difference between (1) and (3) is that the latter is an expectation of the loss $\mathcal{L}(\phi_\theta(t))$ with respect to a uniform distribution on $t \in [0, 1]$, while (1) is an expectation with respect to a uniform distribution on the curve. The two losses coincide, for example, when $\phi_\theta(\cdot)$ defines a polygonal chain with two line segments of equal length and the parametrization of each of the two segments is linear in t .

To minimize (3), at each iteration we sample $t \in [0, 1]$ from the uniform distribution and make a gradient step for θ with respect to the loss $\mathcal{L}(\phi_\theta(t))$. This way we obtain unbiased estimates of the gradients of $\ell(\theta)$, as

$$\mathbb{E}_{t \sim U(0,1)} \nabla_\theta \mathcal{L}(\phi_\theta(t)) = \nabla_\theta \mathbb{E}_{t \sim U(0,1)} \mathcal{L}(\phi_\theta(t)) = \nabla_\theta \ell(\theta).$$

We repeat these updates until convergence.

3.2. Example Parametrizations

3.2.1. POLYGONAL CHAIN

The simplest parametric curve we consider is the polygonal chain (see Figure 1, right). The trained networks \hat{w}_1 and \hat{w}_2 serve as the endpoints of the chain and the bends of the chain are the parameters θ of the curve parametrization. Consider the simplest case of a chain with one bend θ . Then

$$\phi_\theta(t) = \begin{cases} 2(t\theta + (0.5 - t)\hat{w}_1), & 0 \leq t \leq 0.5 \\ 2((t - 0.5)\hat{w}_2 + (1 - t)\theta), & 0.5 \leq t \leq 1. \end{cases}$$

These formulas naturally generalize for n bends $\theta = \{w_1, w_2, \dots, w_n\}$ (see Appendix).

3.2.2. BEZIER CURVE

A Bezier curve (see Figure 1, middle) provides a convenient parametrization of smooth paths with given endpoints. A quadratic Bezier curve $\phi_\theta(t)$ with endpoints \hat{w}_1 and \hat{w}_2 is given by

$$\phi_\theta(t) = (1 - t)^2 \hat{w}_1 + 2t(1 - t)\theta + t^2 \hat{w}_2, \quad 0 \leq t \leq 1.$$

The formulas can be extended to the higher-order case (see Appendix).

3.3. Batch Normalization

Batch normalization (Ioffe & Szegedy (2015)) is essential to modern deep learning architectures. Batch normalization re-parametrizes the output of each layer as

$$\hat{x} = \gamma \frac{x - \mu(x)}{\sigma(x) + \epsilon} + \beta,$$

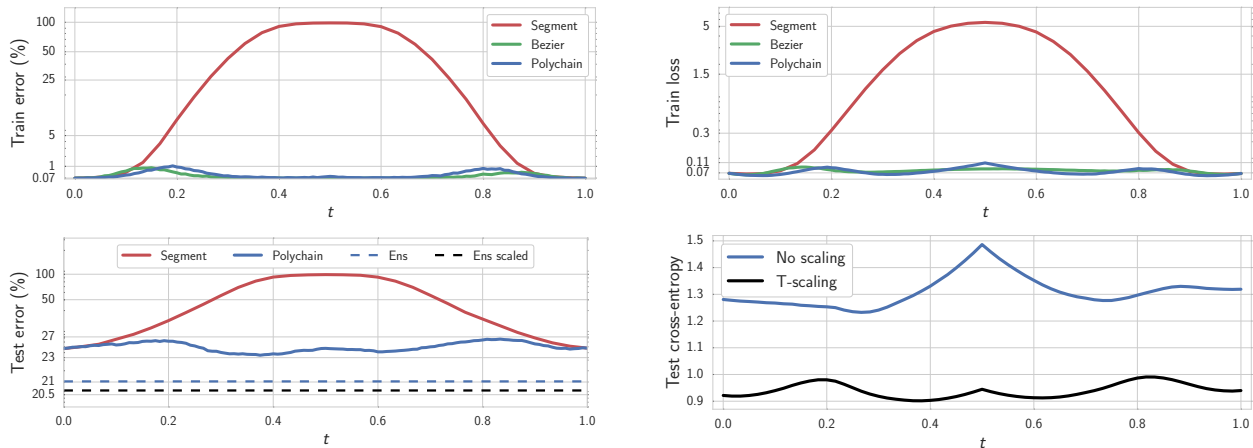


Figure 2. Error as a function of the point on the curves $\phi_\theta(t)$ found by the proposed method, using a ResNet-164 on CIFAR-100. **Top left:** train error. **Bottom left:** test error; dashed lines correspond to quality of ensemble constructed from curve points before and after logits rescaling. **Top right:** train loss (ℓ_2 regularized cross-entropy). **Bottom right:** cross-entropy before and after logits rescaling for the polygonal chain.

where $\mu(x)$ and $\sigma(x)$ are the mean and standard deviation of the output x , $\epsilon > 0$ is a constant for numerical stability and γ and β are free parameters. During training, $\mu(x)$ and $\sigma(x)$ are computed separately for each mini-batch and at test time statistics aggregated during training are used.

When connecting two DNNs that use batch normalization, along a curve $\phi(t)$, we compute $\mu(x)$ and $\sigma(x)$ for any given t over mini-batches during training, as usual. In order to apply batch-normalization to a network on the curve at the test stage we compute these statistics with one additional pass over the data, as running averages for these networks are not collected during training.

4. Curve Finding Experiments

We show that the proposed training procedure in section 3 does indeed find high accuracy paths connecting different modes, across a range of architectures and datasets. Moreover, we further investigate the properties of these curves, showing that they correspond to meaningfully different representations that can be ensembled for improved accuracy. We use these insights to propose an improved ensembling procedure in section 5, which we empirically validate in section 6.

In particular, we test VGG-16 (Simonyan & Zisserman, 2014) on all datasets, a 28-layer Wide ResNet with widening factor 10 (Zagoruyko & Komodakis, 2016) and a 158-layer ResNet (He et al., 2016) on CIFAR-10, and a 164-layer ResNet-bottleneck (He et al., 2016) on CIFAR-100. For CIFAR-10 and CIFAR-100 we use the same standard data augmentation as Huang et al. (2017). We provide additional results, including experiments for fully connected and recurrent networks, in the Appendix.

For each model and dataset we train two networks with different random initializations to find two modes. Then we use the proposed algorithm of section 3 to find a path connecting these two modes in the weight space with a quadratic Bezier curve and a polygonal chain with one bend. We also connect the two modes with a line segment for comparison. In all experiments we optimize the loss (3), as for Bezier curves the gradient of loss (1) is intractable, and for polygonal chains we found loss (3) to be more stable.

4.1. Curve Evaluation

Figures 1 and 2 show the results of the proposed mode connecting procedure for ResNet-164 on CIFAR-100. Here *loss* refers to ℓ_2 regularized cross-entropy loss. For both the Bezier curve and polygonal chain, train error (Figure 2, top left) and test error (Figure 2, bottom left) are indeed nearly constant, with the Bezier curve performing slightly better than the polygonal chain. On the other hand, the train (Figure 2, top right) and test (Figure 2, bottom right) loss somewhat increase towards $t \approx 0.5$, though the increase is more profound on the test loss. We examine this trend further in section 4.3. In the Appendix, we include a table summarizing all path finding experiments on CIFAR-10 and CIFAR-100 for VGGs, ResNets and Wide ResNets, which follow the same general trends.

We also measured the losses (1) and (3) for all the curves we constructed, and we found that the values of the two losses were very close, suggesting that the loss (3) is a good practical approximation to the loss (1).

The line segments directly connecting two modes generally incur high error. For VGG-16 on CIFAR-10 the test error goes up to 90% in the center of the segment. On the other

hand, for ResNet-158 the worst test error along the segment is 80% for Wide ResNet-28-10 the worst error is just 66%. This finding suggests that the loss surfaces of state-of-the-art residual networks are indeed more regular than those of classical models like VGG, which corresponds with other recent observations (see e.g., Li et al., 2017).

4.2. The Effects of Increasing Parametrization

We investigate the relation between the observed connectedness of the local optima and the number of parameters (weights) in the neural network. We start with a network that has three convolutional layers followed by three fully-connected layers, where each layer has $1000K$ neurons. We vary $K \in \{0.3, 0.5, 0.8, 1\}$, and for each value of K we train two networks that we connect with a Bezier curve using the proposed procedure in section 3.

For each value of K , Figure 3 shows the worst training loss along the curve, maximum of losses of the endpoints, and the ratio of the length of the curve and the line segment connecting the two modes. Increasing the number of parameters we are able to reduce the difference between the worst value of the loss along the curve and the loss of single models used as the endpoints. The ratio of the length of the found curve and the length of the line segment connecting the two modes also decreases monotonically with K . This result is intuitive, since a greater parametrization allows for more flexibility in how we can navigate the loss surfaces. Additionally, in section 4.3 we show that the curves do not correspond to redundancy in the parametrization, since points on the curve can be meaningfully ensembled. In the Appendix we provide a construction that would exploit redundancy in the parametrization to provide curves that correspond to networks that make identical predictions and thus could not be used for ensembling.

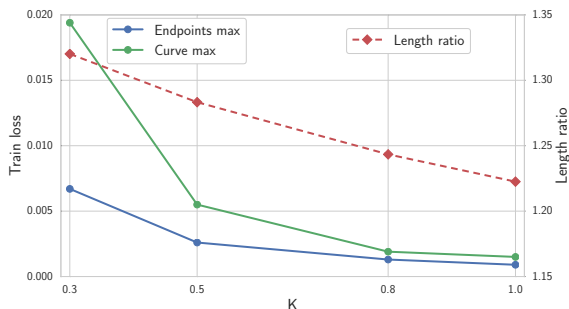


Figure 3. The worst train loss along the curve, maximum of the losses of the endpoints, and the ratio of the length of the curve and the line segment connecting the two modes, as a function of the scaling factor K of the sizes of fully-connected layers.

4.3. Curve Ensembling

Here we explore ensembles constructed from points sampled from these high accuracy curves. In particular, we train a polygonal chain with one bend connecting two independently trained ResNet-164 networks on CIFAR-100 and construct an ensemble of networks corresponding to 50 points placed on an equally-spaced grid on the curve. The resulting ensemble had 21.03% error-rate on the test dataset. The error-rate of the ensemble constructed from the endpoints of the curve was 22.0%. An ensemble of three independently trained networks has an error rate of 21.01%. Thus, the ensemble of the networks on the curve outperformed an ensemble of its endpoints implying that the curves found by the proposed method are actually passing through diverse networks that produce predictions different from those produced by the endpoints of the curve. Moreover, the ensemble based on the polygonal chain has the same number of parameters as three independent networks, and comparable performance.

Furthermore, we can improve the ensemble on the chain without adding additional parameters or computational expense, by accounting for the pattern of increased training and test loss towards the centres of the linear paths shown in Figure 2. While the training and test accuracy are relatively constant, the pattern of loss, shared across train and test sets, indicates overconfidence away from the three points defining the curve: in this region, networks tend to output probabilities closer to 1, sometimes with the wrong answers. This overconfidence decreases the performance of ensembles constructed from the networks sampled on the curves. In order to correct for this overconfidence and improve the ensembling performance we use temperature scaling (Guo et al., 2017), which is inversely proportional to the loss. Figure 2, bottom right, illustrates the test loss of ResNet-164 on CIFAR-100 before and after temperature scaling. After rescaling the predictions of the networks, the test loss along the curve decreases and flattens. Further, the test error-rate of the ensemble constructed from the points on the curve went down from 21.03% to 20.7% after applying the temperature scaling, outperforming 3 independently trained networks.

However, directly ensembling on the curves requires manual intervention for temperature scaling, and an additional pass over the training data for each of the networks (50 in this case) at test time to perform batch normalization as described in section 3.3. Moreover, we also need to train at least two networks for the endpoints of the curve. In section 5 we propose a different ensembling method inspired by the connectedness of the optima that does not have these limitations.

5. Fast Geometric Ensembling

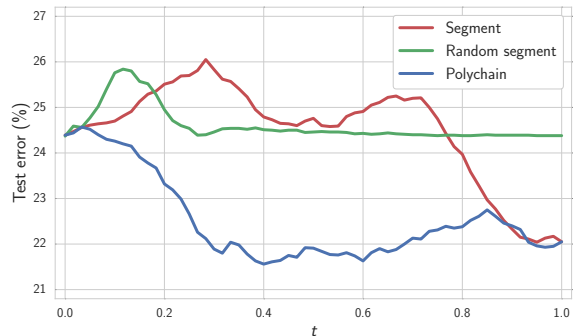


Figure 4. Error of the two-network ensemble consisting of the endpoint of the curve and the point $\phi_\theta(t)$ on the curve (CIFAR-100, ResNet-164). “Segment” is a line segment connecting two modes found by SGD. “Polychain” is a polygonal chain connecting the same endpoints. “Random segment” is a straight line following from the endpoint of the curve in a random direction.

Algorithm 1 Fast Geometric Ensembling

Require:

weights \hat{w} , LR bounds α_1, α_2 ,
 cycle length c (even), number of iterations n

Ensure: ensemble

```

 $w \leftarrow \hat{w}$  {Initialize weight with  $\hat{w}$ }
ensemble  $\leftarrow []$ 
for  $i \leftarrow 1, 2, \dots, n$  do
     $\alpha \leftarrow \alpha(i)$  {Calculate LR for the iteration}
     $w \leftarrow w - \alpha \nabla \mathcal{L}_i(w)$  {Stochastic gradient update}
    if  $\text{mod}(i, c) = c/2$  then
        ensemble  $\leftarrow$  ensemble +  $[w]$  {Collect weights}
    end if
end for
    
```

We introduce a practical ensembling procedure, Fast Geometric Ensembling (FGE), motivated by our observations about mode connectivity.

Let \hat{w}_1 and \hat{w}_2 be two distinct sets of weights corresponding to optima obtained by independently training a DNN two times. In section 4.1 we showed that there exists a path connecting \hat{w}_1 and \hat{w}_2 , such that the test accuracy is high along the path. Let $\phi(t)$, $t \in [0, 1]$ parametrize this path with $\phi(0) = \hat{w}_1$, $\phi(1) = \hat{w}_2$. In section 4.3, we see that ensembling the points on the curve $\phi(\cdot)$ we can achieve improved performance compared to the ensemble of the endpoints \hat{w}_1 and \hat{w}_2 .

We now examine how far we need to move along the curve to find a point that produces substantially different, but still useful, predictions. In particular, we investigate the performance of an ensemble of two networks: the endpoint of the curve and a point $\phi_\theta(t)$ on the curve corresponding to $t \in [0, 1]$. Figure 4 shows the test error of this ensemble as

a function of t , for a ResNet-164 on CIFAR-100. The test error starts going down at $t \approx 0.1$ and for $t \geq 0.4$ the error of an ensemble is approximately the same as the error of an ensemble of the two independently trained networks used as the endpoints of the curve. Thus even by moving away from the endpoint by a relatively small distance along the curve we can find a network that produces meaningfully different predictions from the network at the endpoint. For the line segment connecting the two endpoints of the curve the error only goes down near the second mode, and for a random direction in the weight space the ensemble error never goes below the error of a single network. We observed similar patterns for other architectures.

Suppose now we only have one set of weights \hat{w} corresponding to a mode of the loss. We cannot explicitly construct a path $\phi(\cdot)$ as before, but we know that multiple paths passing through \hat{w} exist, and it is thus possible to move away from \hat{w} in the weight space without increasing the loss. Further, we know that we can find diverse networks providing meaningfully different predictions by making relatively small steps in the weight space.

Inspired by these observations, we propose the Fast Geometric Ensembling (FGE) method that aims to find diverse networks with relatively small steps in the weight space, without leaving a region that corresponds to low test error. Alg. 1 provides an outline of the algorithm. First, we initialize a copy of the network with weights w set equal to the weights of the trained network \hat{w} . Now, to force w to move away from \hat{w} without substantially decreasing the prediction accuracy we adopt a cyclical learning rate schedule, with the learning rate at iteration i defined as

$$\alpha(i) = \begin{cases} (1 - 2t(i))\alpha_1 + 2t(i)\alpha_2 & 0 < t(i) \leq \frac{1}{2} \\ (2 - 2t(i))\alpha_2 + (2t(i) - 1)\alpha_1 & \frac{1}{2} < t(i) \leq 1 \end{cases},$$

where $t(i) = \frac{1}{c}(\text{mod}(i - 1, c) + 1)$, the learning rates are $\alpha_1 > \alpha_2$, and the number of iterations in one cycle is given by c . Here by iteration we mean processing one mini-batch of data. We can train the network w using the standard L_2 -regularized cross-entropy loss function (or any other loss that can be used for DNN training) with the proposed learning rate schedule for n iterations. In the middle of each learning rate cycle when the learning rate reaches its minimum value α_2 (which corresponds to $\text{mod}(i, c) = c/2$) we collect the checkpoints of weights w . When the training is finished we ensemble the collected models.

Figure 5 illustrates the adopted learning rate schedule. During the periods when the learning rate is large (close to α_1), w is exploring the weight space doing larger steps but sacrificing the test error. When the learning rate is small (close to α_2), w is in the exploitation phase in which the steps become smaller and the test error goes down. The cycle length is usually about 2 to 4 epochs, so that the method efficiently

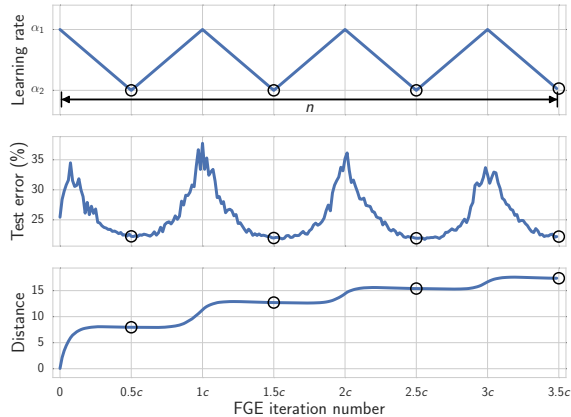


Figure 5. Plot of the learning rate (**Top**), test error (**Middle**) and distance from the initial value (**Bottom**) as a function of iteration for FGE with Preactivation-ResNet-110 on CIFAR-100. Circles indicate the times when we save models for ensembling.

balances exploration and exploitation with relatively-small steps in the weight space that are still sufficient to gather diverse and meaningful networks for the ensemble.

To find a good initialization \hat{w} for the proposed procedure, we first train the network with the standard learning rate schedule (the schedule used to train single DNN models) for about 75% of the time required to train a single model. After this pre-training is finished we initialize FGE with \hat{w} and run the proposed fast ensembling algorithm for the remaining computational budget. In order to get more diverse samples, one can run Algorithm 1 several times for a smaller number of iterations initializing from different checkpoints saved during training of \hat{w} , and then ensemble all of the models gathered across these runs.

Cyclical learning rates have also recently been considered in Smith & Topin (2017) and Huang et al. (2017). Our proposed method is perhaps most closely related to Snapshot Ensembles (Huang et al., 2017), but has several distinctive features, inspired by our geometric insights. In particular, Snapshot Ensembles adopt cyclical learning rates with cycle length on the scale of 20 to 40 epochs from the beginning of the training as they are trying to do large steps in the weight space. However, according to our analysis of the curves it is sufficient to do relatively small steps in the weight space to get diverse networks, so we only employ cyclical learning rates with a small cycle length on the scale of 2 to 4 epochs in the last stage of the training. As illustrated in Figure 5, the step sizes made by FGE between saving two models are on the scale of 7 for Preactivation-ResNet-110 on CIFAR-100. For Snapshot Ensembles for the same model the distance between two snapshots is on the scale of 40. We also use a piecewise linear cyclical learning rate schedule following Smith & Topin (2017) as opposed to the cosine schedule in

Snapshot Ensembles.

6. Fast Geometric Ensembling Experiments

In this section we compare the proposed Fast Geometric Ensembling (FGE) technique against ensembles of independently trained networks (Ind), and SnapShot Ensembles (SSE) (Huang et al., 2017), a recent state-of-the-art fast ensembling approach.

For the ensembling experiments we use a 110-layer Preactivation-ResNet in addition to the VGG-16 and Wide ResNet-28-10 models. Links for implementations to these models can be found in the Appendix. We will release code for FGE upon publication.

We compare the accuracy of each method as a function of computational budget. For each network architecture and dataset we denote the number of epochs required to train a single model as B . For a kB budget, we run each of Ind, FGE and SSE k times from random initializations and ensemble the models gathered from the k runs. In our experiments we set $B = 200$ for VGG-16 and Wide ResNet-28-10 (WRN-28-10) models, and $B = 150$ for ResNet-110, since 150 epochs is typically sufficient to train this model. We note the runtime per epoch for FGE, SSE, and Ind is the same, and so the total computation associated with kB budgets is the same for all ensembling approaches.

For Ind, we use an initial learning rate of 0.1 for ResNet and Wide ResNet, and 0.05 for VGG. For FGE, with VGG we use cycle length $c = 2$ epochs, and a total of 22 models in the final ensemble. With ResNet and Wide ResNet we use $c = 4$ epochs, and the total number of models in the final ensemble is 12 for Wide ResNets and 6 for ResNets. For VGG we set the learning rates to $\alpha_1 = 10^{-2}$, $\alpha_2 = 5 \cdot 10^{-4}$; for ResNet and Wide ResNet models we set $\alpha_1 = 5 \cdot 10^{-2}$, $\alpha_2 = 5 \cdot 10^{-4}$. For both FGE and SSE procedures we run the procedure and average the predictions of the results ensembles. For SSE, we followed Huang et al. (2017) and varied the initial learning rate α_0 and number of snapshots per run M . We report the best results we achieved, which corresponded to $\alpha_0 = 0.1$, $M = 4$ for ResNet, $\alpha_0 = 0.1$, $M = 5$ for Wide ResNet, and $\alpha_0 = 0.05$, $M = 5$ for VGG. The total number models in the FGE ensemble is constrained by network choice and computational budget. Further experimental details are in the Appendix.

Table 1 summarizes the results of the experiments. In all conducted experiments FGE outperforms SSE, particularly as we increase the computational budget. The performance improvement against Ind is most noticeable for CIFAR-100. With a large number of classes, any two models are less likely to make the same predictions. Moreover, there will be greater uncertainty over which representation one should use on CIFAR-100, since the number of classes is increased

Table 1. Error rates (%) on CIFAR-100 and CIFAR-10 datasets for different ensembling techniques and training budgets. The best results for each dataset, architecture, and budget are **bolded**.

DNN (Budget)	method	CIFAR-100			CIFAR-10		
		1 Budget	2 Budgets	3 Budgets	1 Budget	2 Budgets	3 Budgets
VGG-16 (200)	Ind	27.4	25.28	24.45	6.81	5.89	5.9
	SSE	26.4	25.16	24.69	6.5	6.19	5.95
	FGE	25.74	24.11	23.54	6.48	5.82	5.66
ResNet-110 (150)	Ind	21.37	19.04	18.59	4.7	4.1	3.77
	SSE	20.75	19.28	18.91	4.66	4.37	4.3
	FGE	20.16	18.67	18.21	4.55	4.21	3.98
WRN-28-10 (200)	Ind	19.1	17.48	17.01	3.74	3.4	3.31
	SSE	17.78	17.3	16.97	3.74	3.54	3.55
	FGE	17.73	16.95	16.88	3.64	3.38	3.52

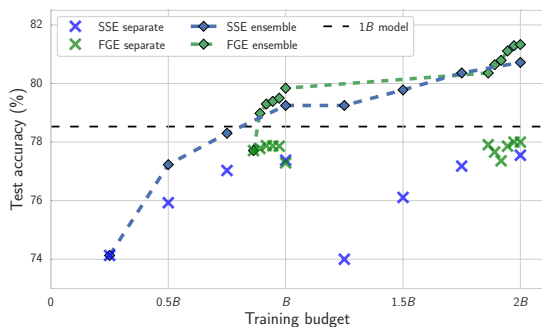


Figure 6. Ensemble performance of FGE (Geometric Fast Ensembling) and SSE (Snapshot Ensembles) as a function of training time, using ResNet-110 on CIFAR-100 ($B = 150$ epochs). Crosses represent the performance of separate “snapshot” models, and diamonds show the performance of the ensembles constructed of all models available by the given time.

tenfold from CIFAR-10, but the number of training examples is held constant. Thus smart ensembling strategies will be especially important on this dataset. Indeed in all experiments on CIFAR-100, FGE outperformed all other methods. On CIFAR-10, FGE consistently improved upon SSE for all budgets and architectures. FGE also improved against Ind for all training budgets with VGG, but is more similar in performance to Ind on CIFAR-10 when using ResNets.

Figure 6 illustrates the results for Preactivation-ResNet-110 on CIFAR-100 for one and two training budgets. Snapshot Ensembles use a cyclical learning rate from the beginning of the training and they gather the models for the ensemble throughout training. To find a good initialization we run standard independent training for the first 75% of epochs (in this case 125 epochs) before applying FGE, as described in section 5 and the supplement. In this case, the whole ensemble is gathered over the last 22 epochs of each of the two runs. During these 22 epochs FGE is able to gather diverse enough networks to outperform Snapshot Ensembles

both for $1B$ and $2B$ budgets.

6.1. ImageNet

ImageNet ILSVRC-2012 (Russakovsky et al., 2012) is a largescale dataset containing 1.2 million training images and 50000 validation images divided into 1000 classes.

CIFAR-100 is the primary focus of our ensemble experiments. However, we also include ImageNet results for the proposed FGE procedure, using a ResNet-50 architecture. We used a pretrained model with top-1 test error of 23.87 to initialize the FGE procedure. We then ran FGE for 5 epochs with a cycle length of 2 epochs and with learning rates $\alpha_1 = 10^{-3}$, $\alpha_2 = 10^{-5}$. The top-1 test error-rate of the final ensemble was 23.31. Thus, in just 5 epochs we could improve the accuracy of the model by 0.56 using FGE. The final ensemble contains 4 models (including the pretrained one). Despite the harder setting of only 5 epochs to construct an ensemble, FGE performs comparably to the best result reported by Huang et al. (2017) on ImageNet, 23.33 error, which was also achieved using a ResNet-50.

7. Discussion and Future Work

We have shown that the optima of deep neural networks are connected by simple pathways, such as a polygonal chain with a single bend, with near constant accuracy. We introduced a training procedure to find these pathways, with a user-specific curve of choice. We were inspired by these insights to propose a practical new ensembling approach, Fast Geometric Ensembling, which achieves state-of-the-art results on CIFAR-10, CIFAR-100, and ImageNet.

There are so many exciting future directions for this research. At a high level we have shown that even though the loss surfaces of deep neural networks are very complex, there is relatively simple structure connecting different optima. Indeed, we can now move towards thinking about valleys of low loss, rather than isolated modes.

These valleys could inspire new directions for approximate Bayesian inference, such as stochastic MCMC approaches which could now jump along these bridges between modes, rather than getting stuck exploring a single mode. One could similarly derive new proposal distributions for variational inference, exploiting the flatness of these pathways. These geometric insights could also be used to accelerate the convergence, stability and accuracy of optimization procedures like SGD, by helping us understand the trajectories along which the optimizer moves, and making it possible to develop procedures which can now search in more structured spaces of high accuracy. One could also use these paths to construct methods which are more robust to adversarial attacks, by using an arbitrary collection of diverse models described by a high accuracy curve, returning the predictions of a different model for each query from an adversary. We can also use this new property to create better visualizations of multilayer loss surfaces. Indeed, using the proposed training procedure, we were able to produce new types of visualizations showing the connectivity of modes, which are normally depicted as isolated. We also could continue to build on the new training procedure we proposed here, to find curves with particularly desirable properties, such as diversity of networks. Indeed, we could start to use entirely new loss functions, such as line and surface integrals of cross-entropy across structured regions of weight space.

Acknowledgements. This work was supported by NSF IIS-1563887, Samsung Research, Samsung Electronics and Russian Science Foundation grant 17-11-01027.

References

- Abadi, Martín, Agarwal, Ashish, Barham, Paul, Brevdo, Eugene, Chen, Zhifeng, Citro, Craig, Corrado, Greg S, Davis, Andy, Dean, Jeffrey, Devin, Matthieu, et al. Tensorflow: Large-scale machine learning on heterogeneous distributed systems. *arXiv preprint arXiv:1603.04467*, 2016.
- Auer, Peter, Herbster, Mark, and Warmuth, Manfred K. Exponentially many local minima for single neurons. In *Advances in neural information processing systems*, pp. 316–322, 1996.
- Choromanska, Anna, Henaff, Mikael, Mathieu, Michael, Arous, Gérard Ben, and LeCun, Yann. The loss surfaces of multilayer networks. In *Artificial Intelligence and Statistics*, pp. 192–204, 2015.
- Dauphin, Yann N, Pascanu, Razvan, Gulcehre, Caglar, Cho, Kyunghyun, Ganguli, Surya, and Bengio, Yoshua. Identifying and attacking the saddle point problem in high-dimensional non-convex optimization. In *Advances in neural information processing systems*, pp. 2933–2941, 2014.
- Dinh, Laurent, Pascanu, Razvan, Bengio, Samy, and Bengio, Yoshua. Sharp minima can generalize for deep nets. In Precup, Doina and Teh, Yee Whye (eds.), *Proceedings of the 34th International Conference on Machine Learning*, volume 70 of *Proceedings of Machine Learning Research*, pp. 1019–1028, International Convention Centre, Sydney, Australia, 06–11 Aug 2017. PMLR. URL <http://proceedings.mlr.press/v70/dinh17b.html>.
- Draxler, F., Veschgini, K., Salmhofer, M., and Hamprecht, F. A. Essentially No Barriers in Neural Network Energy Landscape. *arXiv preprint*, 2018.
- Freeman, C Daniel and Bruna, Joan. Topology and geometry of half-rectified network optimization. *International Conference on Learning Representations*, 2017. URL <https://openreview.net/forum?id=Bk0FWVcgx>.
- Goodfellow, Ian J, Vinyals, Oriol, and Saxe, Andrew M. Qualitatively characterizing neural network optimization problems. *International Conference on Learning Representations*, 2015.
- Guo, Chuan, Pleiss, Geoff, Sun, Yu, and Weinberger, Kilian Q. On calibration of modern neural networks. In *International Conference on Machine Learning*, pp. 1321–1330, 2017.
- He, Kaiming, Zhang, Xiangyu, Ren, Shaoqing, and Sun, Jian. Deep residual learning for image recognition. In *Proceedings of the IEEE conference on computer vision and pattern recognition*, pp. 770–778, 2016.
- Hochreiter, Sepp and Schmidhuber, Jürgen. Flat minima. *Neural Computation*, 9(1):1–42, 1997.
- Huang, Gao, Li, Yixuan, Pleiss, Geoff, Liu, Zhuang, Hopcroft, John E, and Weinberger, Kilian Q. Snapshot ensembles: Train 1, get m for free. *arXiv preprint arXiv:1704.00109*, 2017.
- Ioffe, Sergey and Szegedy, Christian. Batch normalization: Accelerating deep network training by reducing internal covariate shift. In *International Conference on Machine Learning*, pp. 448–456, 2015.
- Jonsson, Hannes, Mills, Greg, and Jacobsen, Karsten W. Nudged elastic band method for finding minimum energy paths of transitions. *Classical and quantum dynamics in condensed phase simulations*, 1998.

Keskar, Nitish Shirish, Mudigere, Dheevatsa, Nocedal, Jorge, Smelyanskiy, Mikhail, and Tang, Ping Tak Peter. On large-batch training for deep learning: Generalization gap and sharp minima. *International Conference on Learning Representations*, 2017. URL <https://openreview.net/references/pdf?id=H1oyRlYgg>.

Lee, Jason D, Simchowitz, Max, Jordan, Michael I, and Recht, Benjamin. Gradient descent only converges to minimizers. In *Conference on Learning Theory*, pp. 1246–1257, 2016.

Li, Hao, Xu, Zheng, Taylor, Gavin, and Goldstein, Tom. Visualizing the loss landscape of neural nets. *arXiv preprint arXiv:1712.09913*, 2017.

Loshchilov, Ilya and Hutter, Frank. Sgdr: Stochastic gradient descent with warm restarts. 2016.

Marcus, Mitchell P, Marcinkiewicz, Mary Ann, and Santorini, Beatrice. Building a large annotated corpus of english: The penn treebank. *Computational linguistics*, 19(2):313–330, 1993.

Russakovsky, Olga, Deng, Jia, Su, Hao, Krause, Jonathan, Satheesh, Sanjeev, Ma, Sean, Huang, Zhiheng, Karpathy, Andrej, Khosla, Aditya, Bernstein, Michael, et al. Imagenet large scale visual recognition challenge. *International Journal of Computer Vision*, 115(3):211–252, 2012.

Simonyan, Karen and Zisserman, Andrew. Very deep convolutional networks for large-scale image recognition. *arXiv preprint arXiv:1409.1556*, 2014.

Smith, Leslie N and Topin, Nicholas. Exploring loss function topology with cyclical learning rates. *arXiv preprint arXiv:1702.04283*, 2017.

Xie, Jingjing, Xu, Bing, and Chuang, Zhang. Horizontal and vertical ensemble with deep representation for classification. *arXiv preprint arXiv:1306.2759*, 2013.

Zagoruyko, Sergey and Komodakis, Nikos. Wide residual networks. *arXiv preprint arXiv:1605.07146*, 2016.

A. Appendix

This Appendix is organized as follows. Section A.1 provides formulas for a polygonal chain and Bezier curve with n bends. Section A.2 discusses the computational complexity of the proposed curve finding method. Section A.3 provides details and results of additional experiments on curve finding. Section A.4 provides visualizations of the train loss and test accuracy surfaces. Section A.5 provides details of experiments on FGE. Finally, section A.6 discusses a trivial

construction of curves connecting two modes, where each point on the curve corresponds to the same representation, unlike the curves in the main text.

A.1. Formulas for curves with n bends

For n bends $\theta = \{w_1, w_2, \dots, w_n\}$, the parametrization of a polygonal chain connecting points w_0, w_{n+1} is given by

$$\phi_\theta(t) = (n+1) \cdot \left(\left(t - \frac{i}{n+1} \right) \cdot w_{i+1} + \left(\frac{i+1}{n+1} - t \right) \cdot w_i \right),$$

for $\frac{i}{n+1} \leq t \leq \frac{i+1}{n+1}$ and $0 \leq i \leq n$.

For n bends $\theta = \{w_1, w_2, \dots, w_n\}$, the parametrization of a Bezier curve connecting points w_0 and w_{n+1} is given by

$$\phi_\theta(t) = \sum_{i=0}^{n+1} w_i C_{n+1}^i t^i (1-t)^{n+1-i}$$

A.2. Computational complexity of curve finding

The forward pass of the proposed method consists of two steps: computing the point $\phi_\theta(t)$ and then passing a mini-batch of data through the DNN corresponding to this point. Similarly, the backward pass consists of first computing the gradient of the loss with respect to $\phi_\theta(t)$, and then multiplying the result by the Jacobian $\frac{\partial \phi_\theta}{\partial \theta}$. The second step of the forward pass and the first step of the backward pass are exactly the same as the forward and backward pass in the training of a single DNN model. The additional computational complexity of the procedure compared to single model training comes from the first step of the forward pass and the second step of the backward pass and in general depends on the parametrization $\phi_\theta(\cdot)$ of the curve.

In our experiments we use curve parametrizations of a specific form. The general formula for a curve with one bend is given by

$$\phi_\theta(t) = \hat{w}_1 \cdot c_1(t) + \theta \cdot c(t) + \hat{w}_2(t) \cdot c_2(t).$$

Here the parameters of the curve are given by $\theta \in \mathbb{R}^{|net|}$.

For this family of curves the computational complexity of the first step of the method is $\mathcal{O}(|net|)$, as we only need to compute a weighted sum of \hat{w}_1 , \hat{w}_2 and $\theta \in \mathbb{R}^{|net|}$. The Jacobian matrix

$$\frac{\partial \phi_\theta(t)}{\partial \theta} = c(t) \cdot I,$$

thus the additional computational complexity of the backward pass is also $\mathcal{O}(|net|)$, as we only need to multiply the gradient with respect to $\phi_\theta(t)$ by a constant. Thus, the total additional computational complexity is $\mathcal{O}(|net|)$. In practice we observe that the gap in time-complexity between one

epoch of training a single model and one epoch of the proposed method with the same network architecture is usually below 15%.

A.3. Curve Finding Experiments

All experiments on curve finding were conducted with TensorFlow (Abadi et al. (2016)) and as baseline models we used the following implementations:

- ResNet-bottleneck-164 and Wide ResNet-28-10 (<https://github.com/tensorflow/models/tree/master/research/resnet>);
- ResNet-158 (<https://github.com/tensorflow/models/tree/master/official/resnet>);
- A reimplementation of VGG-16 without batch-normalization from (<https://github.com/pytorch/vision/blob/master/torchvision/models/vgg.py>);

Table 2 summarizes the results of the curve finding experiments with all datasets and architectures. For each of the models we report the properties of train loss and the error on the train and test datasets. For each of these metrics we report 3 values: “Max” is the maximum values of the metric along the curve, “Int” is a numerical approximation of the integral $\int \langle \text{metric} \rangle (\phi_\theta) d\phi_\theta / \int d\phi_\theta$, where $\langle \text{metric} \rangle$ represents the train loss or the error on the train or test dataset and “Min” is the minimum value of the error on the curve. “Int” represents a mean over a uniform distribution on the curve, and for the train loss it coincides with the loss (1) in the paper. We use an equally-spaced grid with 121 points on $[0, 1]$ to estimate the values of “Min”, “Max”, “Int”. For “Int” we use the trapezoidal rule to estimate the integral. For each dataset and architecture we report the performance of single models used as the endpoints of the curve as “Single”, the performance of a line segment connecting the two single networks as “Segment”, the performance of a quadratic Bezier curve as “Bezier” and the performance of a polygonal chain with one bend as “Polychain”. Finally, for each curve we report the ratio of its length to the length of a line segment connecting the two modes.

We also examined the quantity “Mean” defined as $\int \langle \text{metric} \rangle (\phi_\theta) d\theta$, which coincides with the loss (3) from the paper, but in all our experiments it is nearly equal to “Int”.

Besides convolutional and fully-connected architectures we also apply our approach to RNN architecture on next word prediction task, PTB dataset (Marcus et al. (1993)). As a base model we used the implementation available at <https://www.tensorflow.org/>

[tutorials/recurrent](#). As the main loss we consider perplexity. The results are presented in Table 3.

A.4. Train loss and test accuracy surfaces

In this section we provide additional visualizations. Fig. 7 and Fig. 8 show visualizations of the train loss and test accuracy for ResNet-164 on CIFAR-100 and VGG-16 on CIFAR-10.

A.5. Fast geometric ensembling experiments

As baseline models we used the following implementations:

- VGG-16 (<https://github.com/pytorch/vision/blob/master/torchvision/models/vgg.py>);
- Preactivation-ResNet-110 (<https://github.com/bearpaw/pytorch-classification/blob/master/models/cifar/preresnet.py>);
- ResNet-50 ImageNet (<https://github.com/pytorch/vision/blob/master/torchvision/models/resnet.py>);
- Wide ResNet-28-10 (https://github.com/meliketoy/wide-resnet.pytorch/blob/master/networks/wide_resnet.py);

For the FGE (Fast Geometric Ensembling) strategy on ResNet we run the FGE routine summarized in Alg. 1 after epoch 125 of the usual (same as Ind) training for 22 epochs. The total training time is thus $125 + 22 = 147$ epochs. For VGG and Wide ResNet models we run the pre-training procedure for 156 epochs to initialize FGE. Then we run FGE for 22 epochs starting from checkpoints corresponding to epochs 120 and 156 and ensemble all the gathered models. The total training time is thus $156 + 22 + 22 = 200$ epochs. For VGG we use cycle length $c = 2$ epochs, which means that the total number of models in the final ensemble is 22. For ResNet and Wide ResNet we use $c = 4$ epochs, and the total number of models in the final ensemble is 12 for Wide ResNets and 6 for ResNets.

A.6. Trivial connecting curves

For convolutional networks with ReLU activations and without batch normalization we can construct a path connecting two points in weight space such that the accuracy of each point on the curve (excluding the origin of the weight space) is at least as good as the minimum of the accuracies of the endpoints. Unlike the paths found by our procedure, these paths are trivial and merely exploit redundancies in

Loss Surfaces, Mode Connectivity, and Fast Ensembling of DNNs

Table 2. The properties of loss and error values along the found curves for different architectures and tasks

DNN	Model Curve	Length Ratio	Loss			Train Error (%)			Test Error (%)		
			Min	Int	Max	Min	Int	Max	Min	Int	Max
MNIST											
FC	Single	–	0.018	–	0.0181	0.0117	–	0.0117	1.46	–	1.5
FC	Segment	1	0.018	0.2522	0.6571	0.01	0.53	2.13	1.45	1.96	3.18
FC	Bezier	1.58	0.0157	0.0203	0.0239	0.0117	0.0225	0.035	1.46	1.522	1.56
FC	Polychain	1.73	0.0134	0.0218	0.029	0	0.03	0.07	1.46	1.51	1.58
CIFAR10											
3conv3fc	Single	–	0.0498	–	0.0498	0.06	–	0.06	12.3	–	12.36
3conv3fc	Segment	1	0.494	1.1239	2.4164	0.06	35.69	88.24	12.28	43.3	88.27
3conv3fc	Bezier	1.30	0.0337	0.0377	0.0498	0.05	0.1	0.2	12.06	12.7	13.66
3conv3fc	Polychain	1.67	0.0403	0.0438	0.0498	0.06	0.15	0.31	12.17	12.68	13.31
VGG-16	Single	–	0.0401	–	0.0405	0	–	0.01	6.87	–	7.01
VGG-16	Segment	1	0.0393	1.7586	2.5691	0	61.43	90	6.87	63.75	90
VGG-16	Bezier	1.55	0.0276	0.0303	0.0405	0	0.01	0.02	6.59	6.77	7.01
VGG-16	Polychain	1.83	0.0251	0.0309	0.0445	0	0.01	0.04	6.54	6.89	7.28
ResNet-158	Single	–	0.0150	–	0.0153	0.02	–	0.02	5.56	–	5.74
ResNet-158	Segment	1	0.0133	0.5512	2.613	0.002	16.37	81.41	5.57	20.79	80.00
ResNet-158	Bezier	2.13	0.0133	0.0168	0.0225	0.00	0.02	0.07	5.48	5.82	6.24
ResNet-158	Polychain	3.48	0.0133	0.0168	0.0468	0.00	0.05	0.139	5.48	5.88	7.35
WRN-10-28	Single	–	0.0338	–	0.0349	0	–	0	4.49	–	4.56
WRN-10-28	Segment	1	0.0333	0.412	2.2033	0	5.44	65.62	4.49	10.55	66.6
WRN-10-28	Bezier	1.83	0.0304	0.0329	0.0378	0	0.01	0.04	4.4	4.62	4.83
WRN-10-28	Polychain	1.95	0.0263	0.0291	0.0372	0	0	0	4.38	6.93	10.38
CIFAR100											
VGG-16	Single	–	0.1401	–	0.141	0.05	–	0.06	29.44	–	29.94
VGG-16	Segment	1	0.1374	3.6056	4.9413	0.04	73.25	99	29.44	80.59	99.01
VGG-16	Bezier	1.52	0.0952	0.1069	0.141	0.03	0.08	0.18	29.28	30.49	31.23
VGG-16	Polychain	1.64	0.1184	0.1388	0.1997	0.04	0.19	0.39	29.33	30.13	30.92
ResNet-164	Single	–	0.079	–	0.0799	0.06	–	0.09	24.41	–	24.4
ResNet-164	Segment	1	0.0757	1.8444	5.5289	0.06	38.03	98.65	24.4	53.69	98.83
ResNet-164	Bezier	1.87	0.0736	0.0832	0.0979	0.05	0.28	0.96	24.15	24.99	26.1
ResNet-164	Polychain	2.56	0.0674	0.0778	0.1086	0.06	0.28	0.85	23.98	24.92	26.12

Table 3. The value of perplexity along the found curves for PTB dataset

DNN	Model Curve	Train		Validation		Test	
		Min	Max	Min	Max	Min	Max
PTB							
RNN	Single	37.5	39.2	82.7	83.1	78.7	78.9
RNN	Segment	37.5	596.3	82.7	682.1	78.7	615.7
RNN	Bezier	29.8	39.2	82.7	88.7	78.7	84.0

the parametrization. Also, the training loss goes up substantially along these curves. Below we give a construction of such paths.

Let \hat{w}_1 and \hat{w}_2 be two sets of weights. This path of interest consists of two parts. The first part connects the point \hat{w}_1 with 0 and the second one connects the point \hat{w}_2 with 0. We describe only the first part $\phi(t)$ of the path, such that $\phi(0) =$

$0, \phi(1) = \hat{w}_1$, as the second part is completely analogous. Let the weights of the network \hat{w}_1 be $\{W_i, b_i\}_{1 \leq i \leq n}$ where W_i, b_i are the weights and biases of the i -th layer, and n is the total number of layers. Throughout the derivation we consider the inputs of the network fixed. The output of the i -th layer $o_i = W_i \text{ReLU}(o_{i-1}) + b_i, 1 \leq i \leq n$, where $i = 0$ corresponds to the first layer and $i = n$ corresponds to logits (the outputs of the last layer). We construct $\phi(t) =$

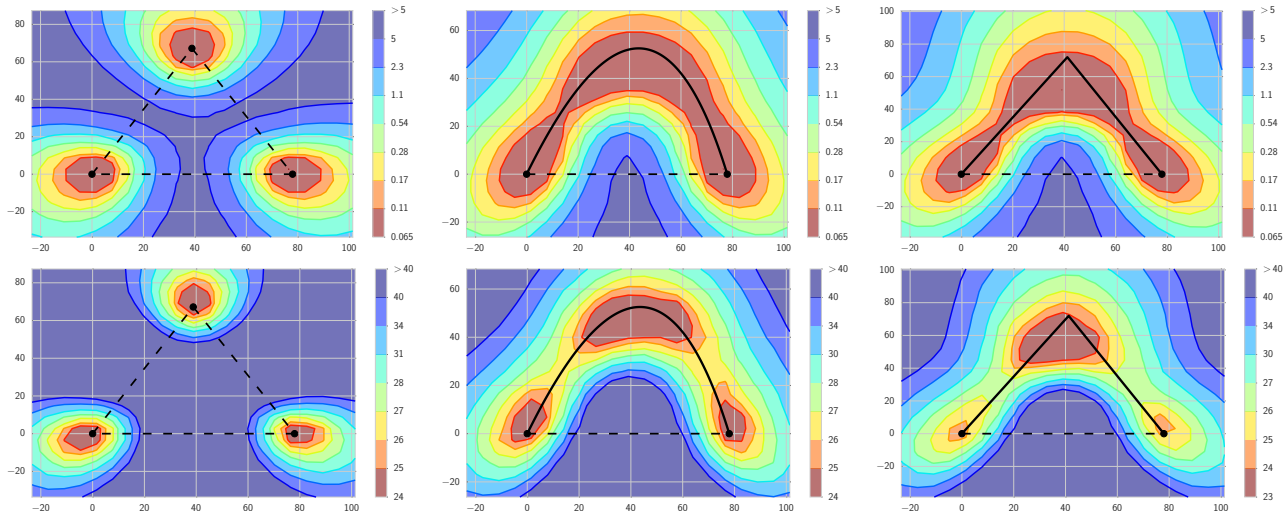


Figure 7. The L_2 -regularized cross-entropy train loss (**Top**) and test error (**Bottom**) surfaces of a deep residual network (ResNet-164) on CIFAR-100. **Left**: Three optima for independently trained networks. **Middle and Right**: A quadratic Bezier curve, and a polygonal chain with one bend, connecting the lower two optima on the left panel along a path of near-constant loss. Notice that in each panel, a direct linear path between each mode would incur high loss.

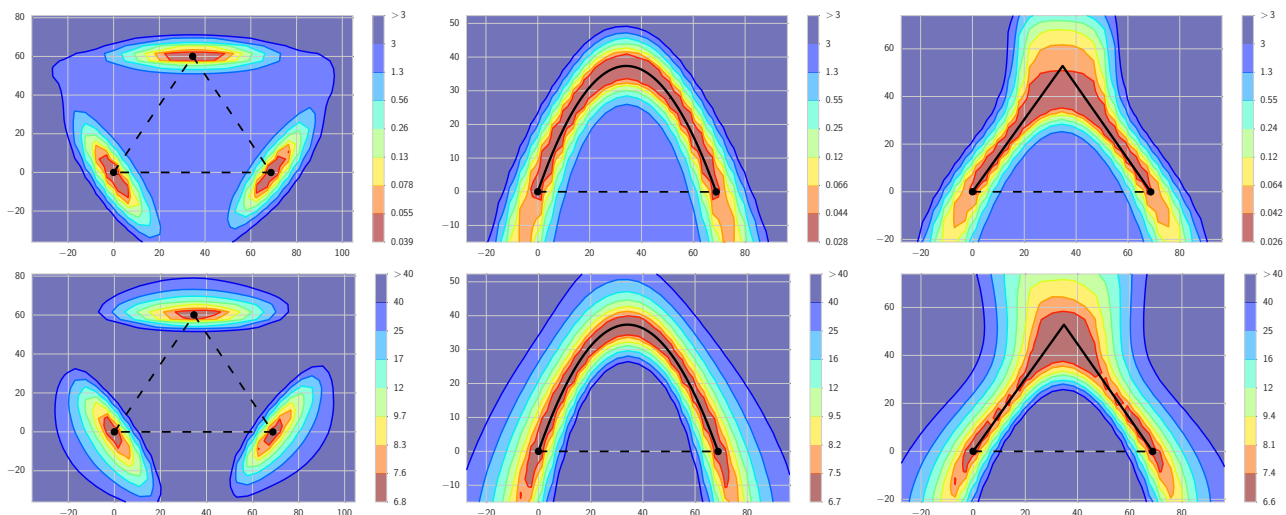


Figure 8. Same as Fig. 7 for VGG-16 on CIFAR-10.

$\{W_i(t), b_i(t)\}_{1 \leq i \leq n}$ in the following way. We set $W_i(t) = W_i t$ and $b_i(t) = b_i t^i$. It is easy to see that logits of the network with weights $\phi(t)$ are equal to $o_n(t) = t^n o_n$ for all $t > 0$. Note that the predicted labels corresponding to the logits $o_n(t)$ and o_n are the same, so the accuracy of all networks corresponding to $t > 0$ is the same.